

RESEARCH ARTICLE

10.1029/2018SW001822

Special Section:

Space Weather Events of 4-10 September 2017

Key Points:

- Analysis of a transformer in New Zealand shows a sequence of large geomagnetically induced currents (GIC) associated with a storm period
- Unique combination of measurements show primarily even harmonics generated by transformer saturation when GIC > 15 A
- During study period only longer-lasting GIC generated observable harmonics but limited GIC impact from impulsive solar wind shock events

Correspondence to:

M. A. Clilverd,
macl@bas.ac.uk

Citation:

Clilverd, M. A., Rodger, C. J., Brundell, J. B., Dalzell, M., Martin, I., Mac Manus, D. H., et al. (2018). Long-lasting geomagnetically induced currents and harmonic distortion observed in New Zealand during the 7–8 September 2017 disturbed period. *Space Weather*, 16. <https://doi.org/10.1029/2018SW001822>

Received 4 FEB 2018

Accepted 19 MAY 2018

Accepted article online 25 MAY 2018

©2018 Crown copyright. This article is published with the permission of the Controller of HMSO and the Queen's Printer for Scotland.

This is an open access article under the terms of the Creative Commons Attribution License, which permits use, distribution and reproduction in any medium, provided the original work is properly cited.

Long-Lasting Geomagnetically Induced Currents and Harmonic Distortion Observed in New Zealand During the 7–8 September 2017 Disturbed Period

Mark A. Clilverd¹, Craig J. Rodger², James B. Brundell², Michael Dalzell³, Ian Martin³, Daniel H. Mac Manus², Neil R. Thomson², Tanja Petersen⁴, and Yuki Obana⁵

¹British Antarctic Survey (NERC), Cambridge, UK, ²Department of Physics, University of Otago, Dunedin, New Zealand, ³Transpower New Zealand Limited, Wellington, New Zealand, ⁴GNS Science, Lower Hutt, New Zealand, ⁵Department of Engineering Science, Osaka Electro-Communication University, Neyagawa, Japan

Abstract Several periods of geomagnetically induced currents (GICs) were detected in the Halfway Bush substation in Dunedin, South Island, New Zealand, as a result of intense geomagnetic storm activity during 6 to 9 September 2017. Unprecedented data coverage from a unique combination of instrumentation is analyzed, that is, measurements of GIC on the single-phase bank transformer T4 located within the substation, nearby magnetic field perturbation measurements, very low frequency (VLF) wideband measurements detecting the presence of power system harmonics, and high-voltage harmonic distortion measurements. Two solar wind shocks occurred within 25 hr, generating four distinct periods of GIC. Two of the GIC events were associated with the arrival of the shocks themselves. These generated large but short-lived GIC effects that resulted in no observable harmonic generation. Nearby and more distant magnetometers showed good agreement in measuring these global-scale magnetic field perturbations. However, two subsequent longer-lasting GIC periods, up to 30 min in duration, generated harmonics detected by the VLF receiver systems, when GIC levels continuously exceeded 15 A in T4. Nearby and more distant magnetometers showed differences in their measurements of the magnetic field perturbations at these times, suggesting the influence of small-scale ionospheric current structures close to Dunedin. VLF receiver systems picked up harmonics from the substation, up to the 30th harmonic, consistent with observed high-voltage increases in even harmonic distortion, along with small decreases in odd harmonic distortion.

1. Introduction

Rapid fluctuations of the Earth's magnetic field can lead to geomagnetically induced currents (GIC) flowing in high-voltage transformers and power systems (Pirjola & Boteler, 2017). Fluctuating ionospheric current systems induce quasi-direct current (DC) in the surface of the Earth, which can enter into man-made transmission lines (Molinski, 2002). The effects of GIC on long transmission lines, such as the early telegraph systems, have been noted since the 1840s (Boteler et al., 1998). Typically the largest GIC levels occur for the fastest rate of change of the geomagnetic field, with the most extreme changes being seen in the region of the auroral electrojet (Birkeland, 1908; Cummings & Dessler, 1967). However, the latitude of the electrojet varies depending on the level of geomagnetic activity (see Oughton et al., 2017, for a comprehensive discussion), with high geomagnetic storming displacing the electrojet equatorward from geomagnetic high latitudes to midlatitudes (Thomson et al., 2011), which would include the southern regions of New Zealand's South Island relevant to this study.

During a GIC event unidirectional DC flux adds to the alternating current flux in transformer cores for alternate half cycles potentially leading to peak magnetic flux levels that drive saturation. This can lead to an increase in the reactive power absorbed by the transformer, potential voltage collapses, and the creation of significant voltage harmonics into the power system (Girgis & Vedante, 2015). Power systems are affected by harmonic distortion through tripping of protective relays, such as those on voltage regulation capacitor banks, which can then result in power outages (Molinski, 2002). Ultimately, the size and impact of induced currents flowing in power systems are a complex interplay between processes driving

geomagnetic field variations (Pulkkinen et al., 2003), the proximity of the power system to the auroral electrojet latitude, the power system network configuration, and the underlying surface conductivity structures (e.g., Divett et al., 2017).

High peak current pulses in transformers generate leakage flux (Albertson et al., 1992) rich in harmonics, increasing winding temperatures through larger eddy current losses in the windings. Heating can also occur in structural parts of a transformer, with tank wall hot spots subject to temperatures as high as 175 °C (Kappenman, 1996). Temperature increases within a transformer are influenced by both the magnitude of the GIC and its duration. Large GIC levels have been observed to flow in power systems as a result of interplanetary solar wind magnetic field (IMF) shock events deforming the Earth's protective geomagnetic field (Fiori et al., 2014; Rodger et al., 2017). The short duration of the high GIC levels in IMF shock cases would be expected to cause significantly smaller temperature increases in transformer windings than for longer duration events, potentially limiting the damage or aging of any transformers exposed to these large currents (Viljanen et al., 2001).

Two additional geomagnetic drivers of GIC have been identified: substorms and geomagnetic pulsations. All three drivers involve significant changes in the ground-level magnetic field. Substorms have a peak occurrence around 00 MLT (magnetic local time) and can have durations of about an hour, while geomagnetic pulsations such as ULF Pc5 waves can occur toward the end of a storm period, producing extended GIC periods (several hours) primarily found in the MLT morning period (Pulkkinen et al., 2003). GIC levels associated with geomagnetic pulsations tend to be smaller than those associated with substorms and shocks.

However, the analysis of dissolved gases (DGA) in transformer oils, which can be generated by the breakdown of insulator materials as a result of high operating temperatures, has suggested that there can be accumulative damage to, or aging of, transformers through repeated exposure to GICs (Albertson et al., 1992). Regular checks of DGA from 16 transformers in South Africa showed increased gas levels following two large geomagnetic storms in November 2003 (Gaunt & Coetzee, 2007). Three transformers tripped during the storms, and three were taken out of service several months later with high DGA levels. Inspection showed there was heat damage, mostly to paper insulation, in various parts of the transformers. The damage was initiated by local overheating causing low temperature thermal degradation as set out in Mollman and Pahlavanpour (1999).

The currents of a transformer driven into half cycle saturation contain harmonics of various orders, some even and some odd. Power networks are typically designed to cope with odd harmonics as they are produced by multiple processes. In contrast, even harmonic events are rare and are uniquely produced by GIC (Ramírez-Niño et al., 2016). As such, networks can be stressed by low levels of even harmonics as they are not normally present (Gish et al., 1995). Boteler et al. (1989) presented measurements of increased harmonic currents due to GIC in a 1,200-MVA transformer on the British Columbia Hydro 500-kV system. Measurements were made of the fundamental and second-order harmonics, indicating that during the GIC anticipated odd harmonics produced were by symmetrical saturation, but some very strong low order even harmonics were also generated. The tripping of an overcurrent relay in the Swedish power system during the large geomagnetic storm of October 2003 was triggered by GIC-induced harmonic distortion (Pulkkinen et al., 2005), with the relay being particularly sensitive to the third harmonic. Harmonic distortion data with a time resolution of 1 hr showed a 1.5% peak in the zero-sequence voltage (sum of the fundamental frequency, third, sixth harmonic, etc.) at the time of the power outage. Note that there are currently very few events reported with simultaneous harmonic distortion and GIC measurements.

Enhanced harmonics from nearby power systems have previously been observed with a very low frequency (VLF) receiver during the sudden commencement of a geomagnetic storm as observed in Canada (Hayashi et al., 1978). Enhanced GIC levels giving rise to near saturation of transformer core material were postulated, although no power network current measurements were available at the time. Prior to the storm only odd harmonics were observed, however, following the sudden commencement intense even harmonics up to 720 Hz (twelfth harmonic) appeared as well as some enhancement of the third and ninth harmonics (180 and 520 Hz). Short-lived (tens of seconds) periods with enhanced harmonic amplitude were observed over the following 5 min as damped magnetic field oscillations occurred. The highest even harmonic excited was the eighteenth (1,080 Hz).

Clilverd et al. (2010) correlated the occurrence rate of ~ 1 -s VLF noise bursts with GIC magnitude for a geomagnetic storm in May 2005. The noise bursts observed in northern Finland were observed in the 20- to 25-kHz range and were thought to be generated by nearby electrical arcing caused by the geomagnetic storm. Corroborating wideband VLF data (0.1–30 kHz) were not available at the time, and the correlation with GIC magnitude was from the distant location of Scotland, which merely indicated that the storm was capable of creating GIC. Although power line harmonic radiation has been observed extensively by VLF receivers on the ground and in space (Němec et al., 2006; Yearby et al., 1983), very few VLF wideband spectral observations of GIC transformer saturation effects associated with individual space weather events have been published.

In this study we present observations from the Halfway Bush (HWB) substation in Dunedin, South Island, New Zealand, during 2 days of intense geomagnetic storm activity in September 2017. We combine and interpret a series of measurements made with high time resolution, including GIC measurements made within the substation (Mac Manus et al., 2017), magnetometer measurements made very close to Dunedin, broadband VLF observations made at the substation, and harmonic distortion measurements made on a 110-kV high-voltage line linked to HWB single-phase bank transformer T4. We investigate the impact of short-lived sudden commencement storm effects, along with longer-lasting substorm-like events that produced more significant responses within the substation. We identify GIC levels that produced harmonic distortion, identify the components present, and describe the geomagnetic perturbation characteristics. We suggest that this is an unusually complete set of space weather observations, providing direct evidence of GIC saturation to a transformer, along with measurements of the GIC and resultant harmonics.

2. Experimental Data Sets

The 4–11 September 2017 interval was one of the most flare-productive periods of solar cycle 24. Two active regions produced more than 15 M-class flares, and 3 X-class. A coronal mass ejection associated with a 6 September X9 flare produced severe geomagnetic storming on 7 and 8 September. Two solar wind shock events impacted the magnetosphere, causing rapid fluctuations of the geomagnetic field. Shocks were identified by Solar and Heliospheric Observatory at 23:13 UT on 6 September 2017 and 22:38 UT on 7 September 2017 (<http://umtof.umd.edu/pm/>). With solar wind speeds of 600–700 km/s the propagation time for the shocks to reach the magnetosphere is in the order of ~ 30 min. Figure 1 summarizes the solar wind and geomagnetic conditions for 6 to 10 September 2017 using the DSCOVR measurements made at L1, and ground-based geomagnetic activity measurements. An indication of the levels of geomagnetic substorm activity is given by the Wp index (Nosé et al., 2012), shown in the lower panel of this figure.

The arrival of the first shock late on 6 September can be seen in Figure 1 as a sudden increase in all parameters. This includes IMF B_z , suggesting that the initial disturbance is a sudden impulse rather than a sudden storm commencement and would therefore be only weakly geoeffective as a result (Joselyn & Tsurutani, 1990). During the first few hours of 7 September a recovery ensues. The second shock is seen at ~ 23 UT on 7 September, with solar wind speeds exceeding 700 km/s and a very strongly negative IMF B_z . Such shocks are known as sudden storm commencements (SSCs) and are usually geoeffective (Joselyn & Tsurutani, 1990). Finally, at ~ 12 UT on 8 September another strongly negative B_z period is seen, and the solar wind speed remains high (>700 km/s). A steady recovery occurs in all parameters throughout the remainder of 8 September.

2.1. New Zealand GIC Observations

Measurements of transformer DC neutral current have been made at the HWB substation in Dunedin by Transpower New Zealand Limited since an expansion of its monitoring network in the South Island in 2013 (Mac Manus et al., 2017). The substation includes the 50-Hz single-phase bank transformer T4, which was notably damaged by GIC effects on 6 November 2001 (Béland & Small, 2004; Marshall et al., 2012). Neutral currents were monitored using Hall effect current transducers (Liaisons Electroniques-Mécaniques [LEM] model LT 505-S) with typical sampling during a GIC event of 4 s. A detailed description of this data set, along with the corrections to remove stray Earth return currents, was presented by Mac Manus et al. (2017). The HWB T4 GIC observations reported in this study use the corrected data set.

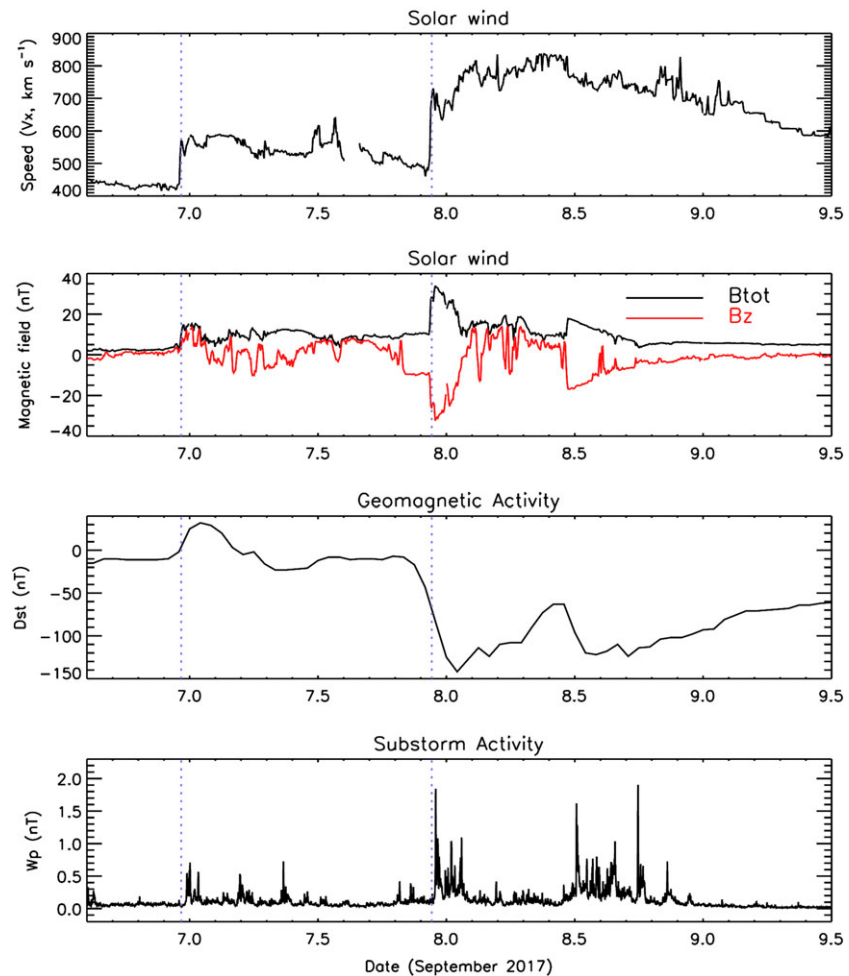


Figure 1. A summary plot of the solar wind and geomagnetic conditions during the disturbed period in September 2017. DSCOVR solar wind speed V_x , and interplanetary magnetic field components (B_{tot} and B_z) are shown in the upper two panels. Geomagnetic activity index Dst and substorm activity index W_p are shown in the lower two panels. Vertical dotted blue lines indicate the times of interplanetary shocks reported by the Solar and Heliospheric Observatory spacecraft.

Total harmonic distortion (THD) measurements were made at circuit breaker CB532, which is connected to HWB T4 and T6 on the 110-kV bus. The percentage of THD for odd and even harmonics on each of the three phases were sampled every 10 min.

2.2. Magnetometers

The proximity of the auroral electrojet is a key factor in the characteristics of the induced currents experienced by power systems (Pulkkinen et al., 2003). Figure 2 shows an image from a Suomi National Polar-orbiting Partnership satellite overpass of New Zealand from 13:36:13 to 13:53:32 UT on 8 September 2017. The map indicates the location of Dunedin in New Zealand and also shows bright auroral features just south of the South Island. The position of the bright auroral features at $\sim 60^\circ\text{S}$ geomagnetic latitude ($L = 4$) in the figure are indicative of the location of the auroral electrojet (Wallis et al., 1976) where its proximity to Dunedin would be anticipated as part of a severe geomagnetic storm period, which displaces the electrojet equatorward (Oughton et al., 2017). Figure 2 also shows the location of the Eyrewell (EYR) magnetometer operated by GNS Science, New Zealand, which is part of INTERMAGNET (<http://www.intermagnet.org/>). EYR is ~ 300 km from Dunedin. A detailed description of the construction of EYR 1-min averages of the horizontal component of the magnetic field is given in Mac Manus et al. (2017), and the data are included in this study to relate the magnetometer measurements for the current time period to previous studies in this region (e.g., Mac Manus et al., 2017; Rodger et al., 2017).

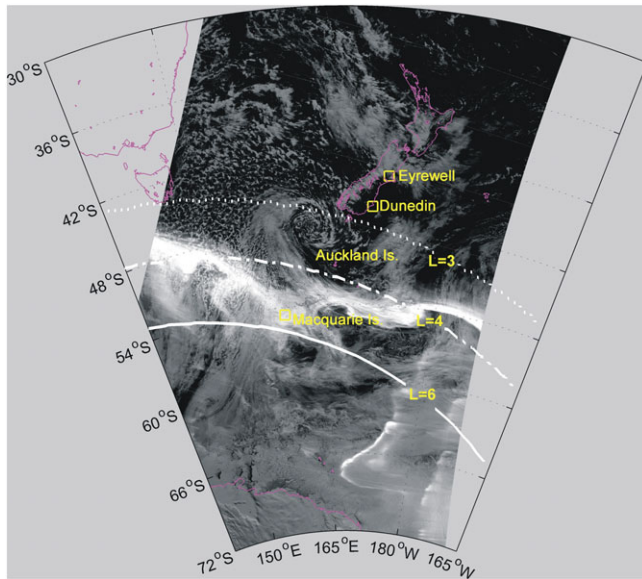


Figure 2. Image provided by a Suomi National Polar-orbiting Partnership satellite overpass of New Zealand, very shortly after the period of peak GIC on 8 September 2017 in the local time early morning. The image was generated by the Near-Constant Contrast product made by the Day/Night Band of the VIIRS sensor. The VIIRS image granules shown here span from 13:36:13 to 13:53:32 UT, with the spacecraft moving north to south. The locations of Eyrewell and Dunedin, South Island, are indicated by squares. Contours of constant geomagnetic latitude are shown as solid, dash-dotted, and dotted lines. VIIRS = Visible Infrared Imaging Radiometer Suite.

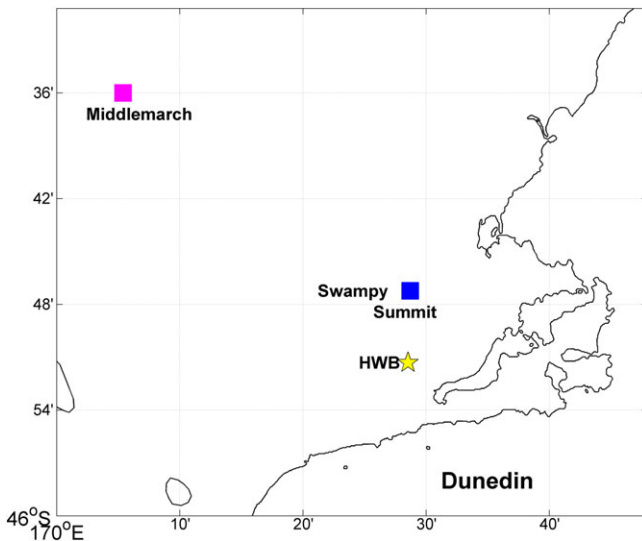


Figure 3. Map of the Dunedin region showing the relative locations of the Halfway Bush (HWB) substation as a yellow star, and the University of Otago research station in the hills of Dunedin at Swampy Summit (blue square). In addition, the Osaka University magnetometer at Middlemarch ~37 km from Swampy is also plotted (magenta square). Note that the overall location of Dunedin is also shown in Figure 2.

In order to compare the HWB T4 GIC observations to changing magnetic field properties associated with the nearby auroral electrojet during the severe geomagnetic storm of 7/8 September 2017, we use local magnetic field measurements made at Swampy Summit close to Dunedin. The locations of the HWB substation (yellow star), and the Swampy Summit (University of Otago) measurement site (blue square) are shown in Figure 3, plotted on a map of the local Dunedin region. The magnetometer at Swampy Summit is a Bartington three-axis magnetic field sensor (MAG-03MSESL70). There is a 7-km separation between the HWB substation and the magnetometer. One-minute average magnetic field component values were calculated in a similar way to those at EYR.

Also shown in Figure 3 is the location of a magnetometer at Middlemarch (purple square), 40 km from the HWB substation. The three-axial fluxgate-type magnetometer is part to the CRUX array (<http://www1.osakac.ac.jp/crux/>) operated by Osaka Electro-Communication University, Japan. It was originally installed in March 2011 with 1-s sampling. The system has been described in Obana et al. (2015).

2.3. VLF Observations

Broadband VLF measurements over the frequency range 0–48 kHz were made at the HWB substation site using two orthogonal vertical magnetic field loop antennas connected to a computer via a sound card as described in Clilverd et al. (2009). Although there were strong local signals from the substation, the gain of the system was set to not overload the aerial preamplifier or the sound card input. The time resolution of the logged data was 10 s, with 46-Hz bins (48-kHz sampling using a 1,024-point Fast Fourier Transform (FFT)). A similar broadband VLF system was also operating at Swampy Summit 7 km away to the north, very close to the site of the Swampy magnetometer. At the Swampy Summit location spectra with 0- to 48-kHz range, 10-s sampling, and 92-Hz resolution were being logged. The two orthogonal VLF aerials at Swampy are orientated in north-south and east-west directions.

3. Magnetic Field and GIC Perturbations

The rate of change of the horizontal magnetic field H component ($H' = dH/dt$) at EYR and Middlemarch for 6 to 9 September 2017 are shown in the upper two panels of Figure 4 (EYR on the top and Middlemarch below). The lower two panels show the Swampy Summit magnetometer H' and HWB T4 GIC for the same period. Four time periods are marked by red lines, based on the times of four distinct peaks in the rate of change of the H component of the EYR data. The times of the peaks are shown in each panel as vertical red lines and marked 1, 2, 3, and 4 in sequence. These four lines are at the following times: (1) 23:48 UT 6 September 2017, (2) 08:56 UT 7 September 2017, (3) 23:02 UT 7 September 2017, and (4) 12:50 UT 8 September 2017.

The four numbered events in EYR H' (upper-middle panel) correspond well with features in either the solar wind or geomagnetic index data, described in section 2. Events 1 and 3 occur at the times of the two solar wind shocks arriving at Earth, with the second one generating significantly larger rates of change at EYR, Middlemarch, and Swampy Summit than the first (~35 nT/min cf. ~7 nT/min). Following both events, the disturbances gradually decline over a period of about 10 hr (the grid

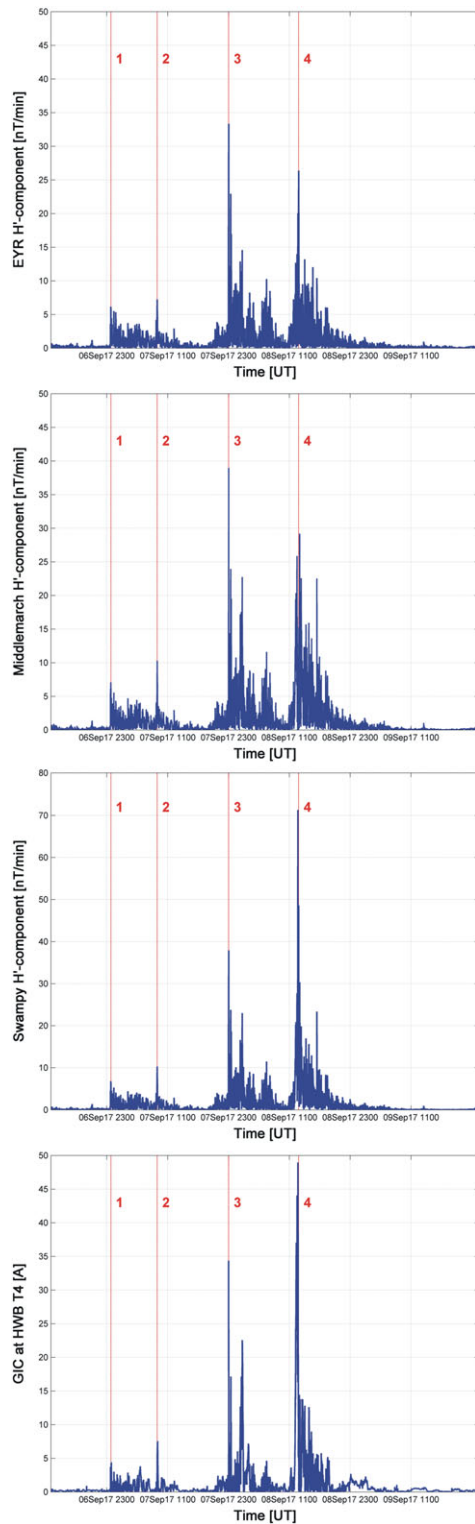


Figure 4. Magnetic field observations from Eyrewell (EYR, first panel), Middlemarch and Swampy Summit (second and third panels), and Halfway Bush (HWB) transformer T4 geomagnetically induced current (GIC) magnitude measurements (lower panel) across the 6–9 September 2017 geomagnetically disturbed period. Four time periods are marked by red lines, based on the times of four distinct peaks in the rate of change of the H component of the EYR data. These times are shown in each panel.

size is 12 hr in the panels). Event 2 is associated with a small substorm following a period of intermittent IMF B_z southward and produces GIC at T4 that are insignificant enough to not be considered further in this study (i.e., ~ 6 A). Event 4 occurs shortly after the strong negative deviation of IMF B_z at ~ 12 UT on 8 September, generating EYR H' rates of change of 26 nT/min, and 29 nT/min at Middlemarch.

The Swampy Summit magnetometer data are shown in the lower left-hand panel of Figure 4. Ostensibly, the Swampy H' look very similar to those from EYR, particularly for events 1, 2, and 3. However, event 4 has a much higher H' (71 nT/min cf. 26 nT/min), and the peak also occurs slightly earlier than at that of EYR (i.e., 9 min beforehand). These observations suggest that event 4 just after 12 UT on 8 September 2017 has localized magnetic field fluctuations closer to Dunedin than Eyrewell, which is consistent with the proximity of the auroral electrojet to Dunedin as identified in Figure 2. This is also consistent with the power grid modeling of Butala et al. (2017), who found that the fidelity between measured GIC levels and modeling using magnetometer proxies is a function of the distance between the two measurements, with shorter separation distances providing more successful modeling outcomes. However, Middlemarch shows a similar peak H' to EYR (29 nT/min cf. 26 nT/m), which is much lower than the Swampy Summit 71 nT/min despite there being only 37 km between the two sites. These observations clearly indicate significant small-scale features in the magnetic field perturbations close to Dunedin, which will be explored in more detail in Figure 5.

The HWB T4 GIC levels show similar characteristics to the Swampy H' , with comparatively small induced current values for events 1 and 2, high levels for event 3, and even higher levels for event 4 (up to ~ 49 A). Taking into account the differences in the three magnetometer sites, these results suggest that event 4 generates large localized fluctuations of the magnetic field and induces large localized currents at the substation. The magnitude of the GIC is similar to those shown for a geomagnetic storm on 2 October 2013 (see Figure 7; Mac Manus et al., 2017), and about half of the peak GIC value thought to have damaged the HWB T4 transformer during a short-duration impulse on 6 November 2001 (Rodger et al., 2017). Following event 4, GIC effects continue to influence T4 for more than 6 hr, gradually subsiding to levels < 5 A.

In Figure 5 we concentrate on the two largest GIC events—event 3 and 4—showing EYR, Swampy Summit, and HWB T4 data, along with the Wp index for the same periods. Here the left-hand column shows observations around event 3 (22:00 UT on 7 September to 03:30 UT on 8 September 2017) and the right-hand column shows the observations around event 4 (10:00 to 15:00 UT on 8 September 2017). As in the previous figure, red lines identify the times of peak H' at EYR. Event 3 is triggered by the L1 solar wind shock at 22:38 UT, which then arrives at Earth at 23:02 UT. The levels of H' at EYR and Swampy are similar (~ 35 nT/min) and occur at the same time, confirming a large-scale perturbation of the magnetosphere as shown by the Dst variation in Figure 1. The ~ 34 -A GIC at T4 lasts only a few minutes, although GIC resulting from further magnetic perturbations continue for several hours at lower levels. From 01:00 to 02:00 UT T4 shows a longer period of enhanced GIC lasting ~ 45 min, exceeding > 15 A for about 5 min at about 01:45 UT. This response would not be predicted through

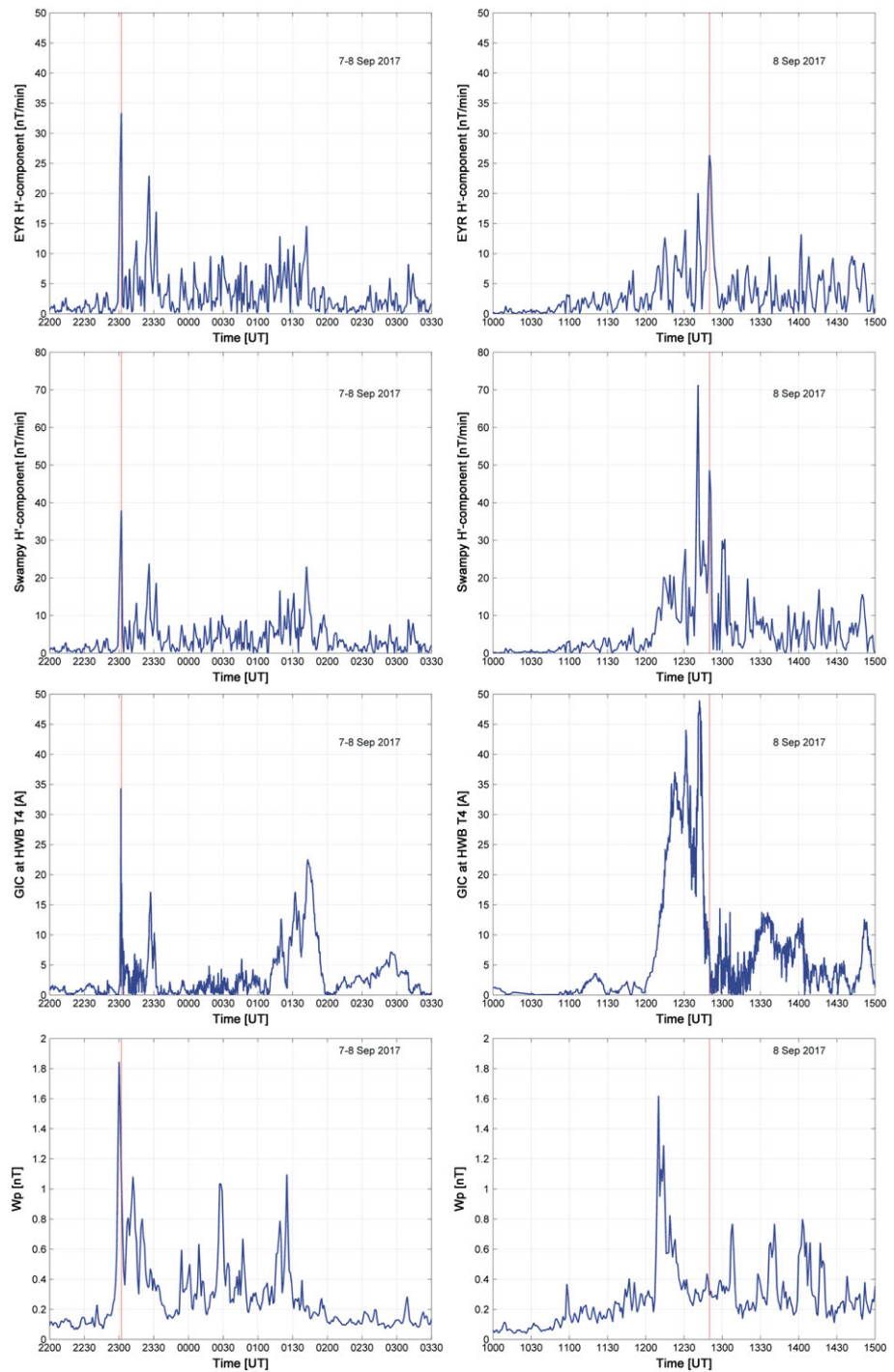


Figure 5. Detailed examination of the magnetic field rate of change and geomagnetically induced current (GIC) variations during the large events 3 (left-hand column) and 4 (right-hand column) identified in Figure 4. Upper panels: Eyrewell (EYR) H' ; middle panels: Swampy Summit H' and Halfway Bush T4 GIC magnitude; lower panel: W_p index. Red lines indicate the times of peaks in H' at EYR. HWB = Halfway Bush.

inspection of the equivalent EYR magnetometer H' data but can be seen as an extended period of relatively high levels of H' at Swampy Summit (>10 nT/min). This enhancement of GIC, occurring about 2 to 3 hr after the arrival of the solar wind shock at 23:02 UT, is consistent with the effects of a geomagnetic substorm (Pulkkinen et al., 2003) as indicated by the W_p index shown in the lower panel. However, the enhancement is probably only noticeable in the Swampy Summit magnetometer H' data because of

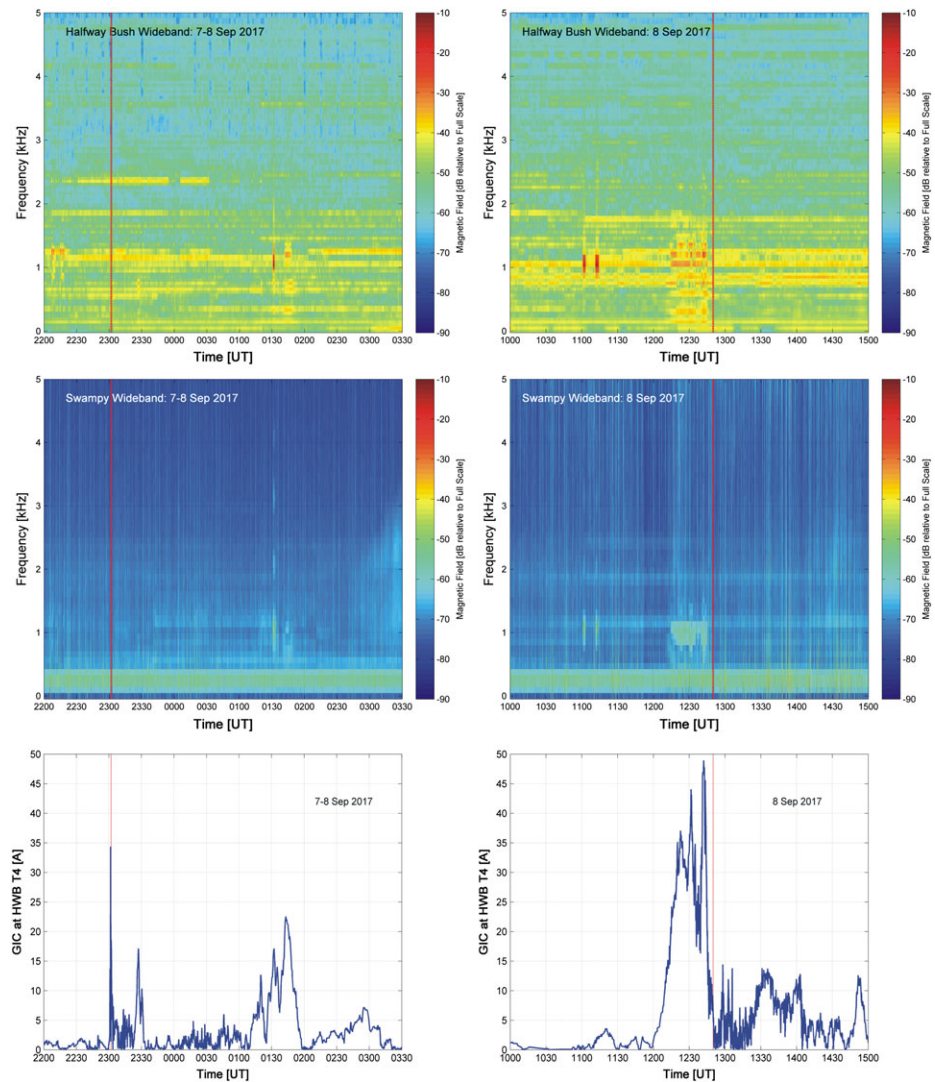


Figure 6. Wideband very low frequency observations from beside the Halfway Bush (HWB) substation and at Swampy Summit north-south aerial. Event 3 is shown in the left column and event 4 is shown in the right column. Periods at about 01:45 UT, and 12:30 UT show evidence of harmonic distortion produced during the high current, long-lasting geomagnetically induced current (GIC) events. HWB GIC data are plotted in the lower panel in order to provide easy comparison with the very low frequency data. Vertical red lines indicate times of large H' at Eyrewell.

Dunedin's proximity to the auroral electrojet, which had been displaced equatorward as a result of the prior shock arrival and the associated negative IMF B_z .

The right-hand column of Figure 5 shows observations made in the time period around event 4 (12:00 to 13:00 UT 8 September 2017). This event is driven by severe geomagnetic storming as indicated by strongly negative IMF B_z and high solar wind speed shown in Figure 1. During this event the transformer T4 experienced long-lasting GIC, with >15 A occurring for ~ 30 min. The timing of the peak current shows good coincidence with the Swampy Summit magnetometer H' , but less so with the more distant EYR magnetometer where the peak in H' is observed ~ 15 min later. The time difference in peak H' between EYR and Swampy Summit appears to stem from differences in the magnitude of short-term variations during the substorm period; that is, EYR shows four peaks in H' increasing in magnitude between 12:00 and 13:00 UT, whereas Swampy Summit shows peaks in H' at the same times but with the third of the four (at $\sim 12:45$ UT) being the largest. This variation in H' responses could be due to the equatorward movement of the electrojet during the substorm, with the distance from EYR decreasing during the substorm time period, and the electrojet passing overhead of Dunedin close to the time of the third peak ($\sim 12:45$ UT). In order to test this idea,

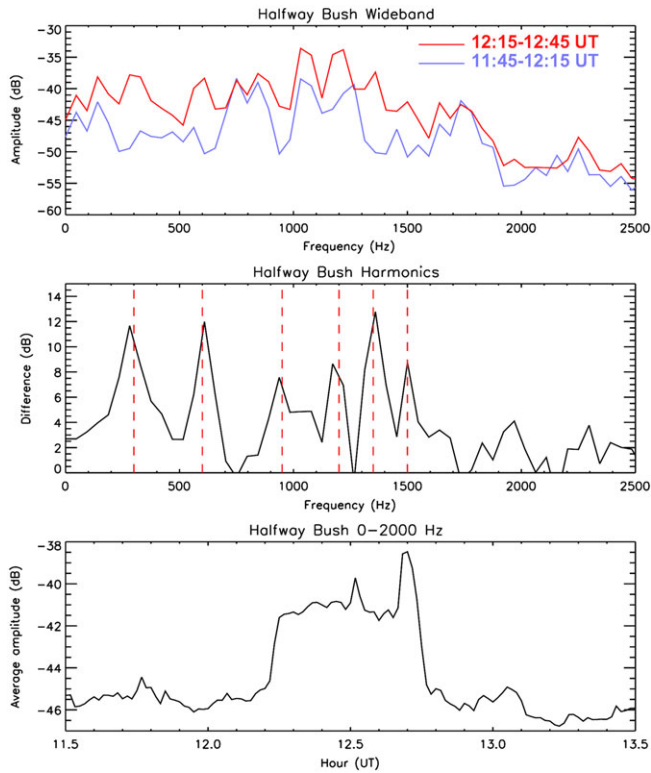


Figure 7. (top panel) Wideband very low frequency observations from the Halfway Bush substation on 8 September 2017, showing the mean amplitude for each frequency bin before (11:45–12:15 UT, blue line) and during (12:15–12:45 UT, red line) the geomagnetically induced current-induced enhanced harmonics period. Increases in harmonics can be seen up to ~1,600 Hz. (middle panel) The difference in received amplitude before and during the geomagnetically induced current > 15 A period. Substantial increases are seen at several frequencies, notably 300, 600, 950, 1,200, 1,350, and 1,500 Hz, while some harmonic frequencies show little change (i.e., 750 and 1,250 Hz). (lower panel) The average intensity of the wideband signal in the range 0–2000 Hz, showing an increase from 12:15 to 12:45 UT.

the event timing of 12–13 UT (01–02 MLT) is consistent with substorm occurrence close to local midnight MLT. This event is the most extreme and long lasting of the GIC recorded at the T4 transformer during the 7/8 September 2017 geomagnetic disturbances.

4. Harmonic Distortion Observations

The broadband VLF magnetic field observations undertaken at the HWB substation showed two periods of enhanced harmonic intensity during the geomagnetic disturbances. The same periods were also detected by a similar broadband VLF system operating at Swampy Summit 7 km away. The observations are shown in Figure 6. The two upper panels show the HWB wideband frequency-time data taken around event 3 on the left (22:00 to 03:30 UT on 7/8 September), and around event 4 on the right (10:00 to 15:00 UT on 8 September). The frequency range is 0–5 kHz, with a frequency resolution of 46 Hz, and 10-s sampling. The color scale represents signal intensity relative to an arbitrary level. As in our previous figures the red vertical lines indicate the times of peak H' at EYR. The middle panels show the same data from Swampy Summit, but at 92-Hz resolution. Many horizontal lines can be seen in all panels. These represent harmonics generated by localized loads on the substation and include three intense pulses at ~1 kHz, which are most likely due to a 1,050-Hz ripple injection system used to control domestic hot water heating systems in the Dunedin area (01:30, 11:00, and 11:15 UT on 8 September). Ripple control in Dunedin was previously described by Werner et al. (2005). However, at 01:45 and 12:30 UT enhancements of harmonics up to 1.6 kHz are seen at HWB, and up to 1 kHz at Swampy Summit. These times are coincident with high GIC levels shown in the

Pearson correlation coefficients were calculated between GIC at HWB and the magnetic field observations. The calculations were performed for event 3 and event 4 separately, using 1-min averaged values. The statistical significance of the Pearson correlation coefficient was examined via the p value (Martin, 2012). For small p values ($p < 0.05$) the null hypothesis may be rejected and the correlation assumed to be statistically significant. For event 3 data were taken from 22:00 to 00:30 UT, 7/8 September 2017. The Pearson correlation coefficient for HWB-EYR was $r = 0.59$ ($p = 10^{-15}$), while for HWB-Swampy Summit $r = 0.60$ ($p = 10^{-16}$). These near-identical results indicate a large-scale perturbation to the magnetic field, which generated similar effects over hundreds of kilometers. For event 4 data were taken from 10:00 to 15:00 UT, 8 September 2017. The Pearson correlation coefficient for HWB-EYR was $r = 0.38$ ($p = 10^{-11}$), while for HWB-Swampy Summit $r = 0.55$ ($p = 10^{-25}$). These results are consistent with small-scale structures being present and a decrease in correlation with increasing distance from HWB. In all of these cases the p values are very close to zero, indicating statistically significant correlations. The Fisher Z test (Preacher, 2002) was also undertaken in order to test whether the differences between the correlation coefficients found using data from the two different magnetometer sites in event 3 are significant, and similarly for event 4. The difference between two independent correlation coefficients are considered significant if $z > \text{modulus}(1.96)$. For event 3, $z = -0.133$ (for 151 data points); that is, there is no significant difference between the two correlation coefficients (0.59 and 0.6). While for the event 4, $z = -2.66$ (for 301 data points); that is, the difference between the correlation coefficients (0.38 and 0.55) is significant. This test confirms that the decrease in correlation with increasing distance from HWB for event 4 is significant.

Unlike the GIC generated by the arrival at Earth of the two solar wind shocks, event 4 shows a gradual enhancement in GIC levels over about 15 min. This enhancement is probably caused by expanding localized ionospheric current systems at ~110 km associated with substorm activity (Pulkkinen et al., 2003) and is coincident with the substorm event that began just after 12 UT as shown by the Wp index in the lower panel. The

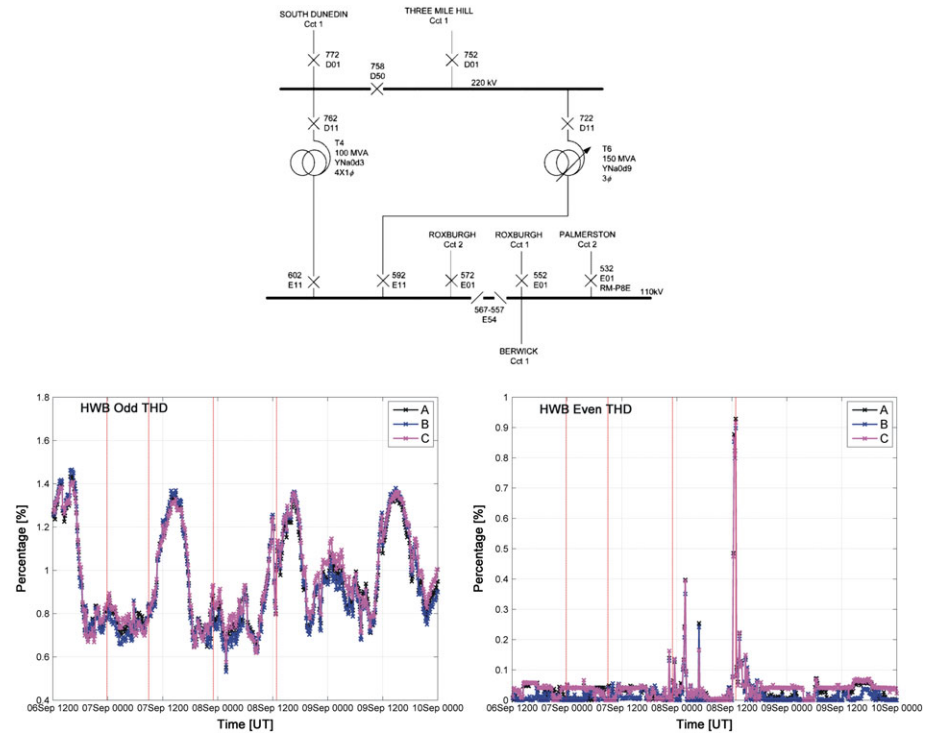


Figure 8. (upper panel) A single line diagram of the Halfway Bush (HWB) substation high-voltage connections, including the circuit breaker CB532 on a 110-kV connection to Palmserston. (lower panels) Total harmonic distortion (THD) measurements made at HWB on a 110-kV line across the 6–9 September 2017 geomagnetically disturbed period. The percentage of THD for odd harmonics (left panel) and even harmonics (right panel) are shown separately. The same four time periods defined from Figure 4 are also indicated. Data representing the red, yellow, and blue phases (denoted as A, B, and C, respectively) are shown.

lower panels. At Swampy Summit the enhanced harmonics were detected in the directional north-south aerial, while nothing was seen in the equivalent east-west aerial. As Swampy Summit is located almost directly north of the HWB substation this observation is regarded as confirmation that the harmonics were detected directly from the substation rather than via transmission through nearby power lines.

The enhanced harmonics observed are closely associated with time periods when transformer T4 experienced greater than ~ 15 A GIC. The duration of the two periods also match the length of time that the GIC exceeds 15 A, that is, 30 min during event 4, and 5 min during the substorm that followed event 3. Notably, event 3 itself, which generated ~ 34 A at 23:00 UT on 7 September shows no evidence of any enhanced harmonics, which is presumably due to the short-lived nature of the shock-induced magnetic field perturbations.

A more detailed analysis of the 8 September 2017 wideband data is shown in Figure 7. The upper panel shows the average amplitude of each 46-Hz frequency bin in the range 0–2,500 Hz for the 30 min period prior to the harmonics being present in event 4 (11:45–12:15 UT) compared with the 30-min period where harmonics were present (12:15–12:45 UT). The panel shows that during event 4 the enhanced harmonics spanned 50–1,600 Hz. The middle panel shows the difference between the two lines presented in the upper panel. Six harmonics that were significantly enhanced during the GIC period are indicated by red vertical dashed lines, that is, the 300- (sixth), 600- (twelfth), 950- (nineteenth), 1,200- (24th), 1,350- (27th), and 1,500-Hz (thirtieth) harmonics. Some harmonics were already present prior to event 4; however, there is little evidence of even harmonics in the VLF spectra, as expected. The harmonics already present included the 750-Hz (fifteenth) harmonic, which showed no change at the time of the enhanced GIC. However, harmonics in the range 950–1,250 Hz were already present and were enhanced during the GIC period. These observations are consistent with previous work (Hayashi et al., 1978) showing the appearance of strong even harmonics (in our case numbers 6, 12, 24, and 30), and the enhancement of some already existing odd harmonics (numbers 19 and 27 in this example) during GIC events.

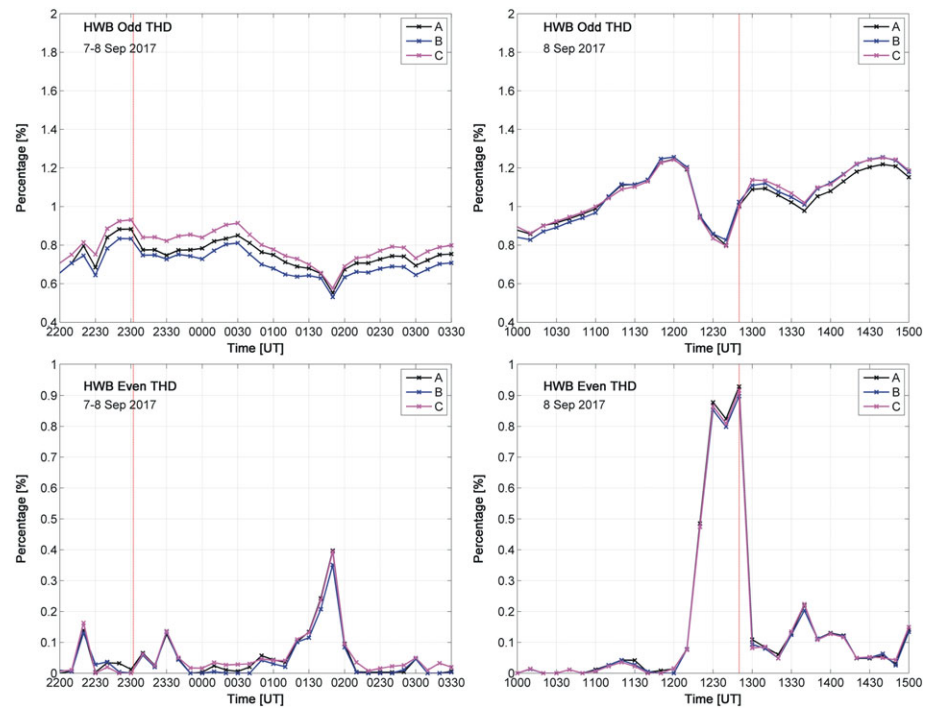


Figure 9. Total harmonic distortion (THD) measurements made at Halfway Bush (HWB) for the voltage on a 110-kV line during the same time periods shown in Figures 4 and 5. The average THD percentage for odd harmonics (upper panels) and even harmonics (lower panels) are shown separately. Data representing the red, yellow, and blue phases (denoted as A, B, and C, respectively) are shown. Vertical red lines indicate times of large H' at Eyrewell.

The lower panel of Figure 7 shows the VLF signal intensity from 0 to 2,000 Hz, averaged with 1-min resolution. The panel shows an increase in intensity above typical background levels, from 12:15 to 12:45 UT, consistent with the T4 GIC levels exceeding 15 A and nonlinear saturation beginning to occur. The temporal variation in 0–2,000 Hz average intensity is also consistent with the variation in T4 GIC levels shown in Figure 5, notably the two peaks that occur at ~12:30 and ~12:45 UT. This suggests a close correlation between the levels of GIC in the substation and the <2 kHz VLF intensity, with the VLF observations also providing harmonic information at the same time.

The strong north-south directionality of the harmonics detected at Swampy Summit, 7 km due north of HWB, suggests that the signals originate from the local distribution network. Harmonic currents can flow in either the transmission system or the local distribution network. Transmission line relative impedance defines, which will happen, particularly in the case of resonant frequencies, which can experience high impedance for certain line lengths. As a result the harmonic current is forced into the on-site distribution network (Carroll et al., 1993). The VLF system appears to have the potential to determine, which harmonics are affected in this way, and the large increase in the amplitude of the 1,350 Hz (27th) harmonic suggests that it is a local resonant frequency.

It is possible to relate the VLF observations of enhanced harmonics from the HWB substation with THD measurements of the 110-kV bus connected to HWB T4, made at circuit breaker CB532 connected to Palmerston. This is depicted in the HWB single line diagram shown in the upper panel of Figure 8, which shows the high-voltage connections at the substation. The lower panels of Figure 8 shows the odd THD (left panel) and the even THD (right panel) for the disturbance period from 12:00 UT, 6 September 2017 to 00:00 UT, 10 September 2017. As before, red vertical lines indicate the event times of peak H' at EYR. The three components of the three-phase electrical power system THD voltage are shown, following the standard naming convention of red, yellow, and blue phases, each alternating current carried by a separate conductor but offset from each other by one third of a cycle (here denoted as A, B, and C, respectively). The odd harmonics show a diurnal variation around 1% distortion, with smaller levels of variability occurring particularly during the daytime in Dunedin (00 UT \pm 6 hr). Small percentage perturbations of the order of 0.1–0.2% occur for the first,

third, and fourth GIC events. Even harmonic THD is rarely above a level of 0.05% but does show peaks that coincide with the third event, the substorm following 3 hr after the third event (about 01:45 UT, 8 September), and very obviously for the fourth event. The largest even THD recorded was $\sim 0.9\%$, while the odd THD at the same time was $\sim 0.8\%$, which should be compared against the steady state upper THD recommendation of 2.5% for 69–161 kV (IEEE Std 519–2014, 2014).

Detailed even and odd THD changes during events 3 and 4 (with the same time ranges as in Figures 4 and 5) are shown in Figure 9. The upper panels show the odd harmonic distortion, while the lower panels show the even harmonic distortion percentages. The red vertical lines indicate the same timing as in previous figures. Event 3 at 23:00 UT on 7 September shows little clear association with any distortion, odd or even, while the substorm at 01:45 UT leads to a decrease in odd distortion of $\sim 0.1\%$ at the same time as an increase to 0.4% in even THD. A similar decrease/increase response can be seen for event 4 at 12:30 UT. Odd THD decreased by $\sim 0.3\%$, while the even THD increased to as much as $\sim 0.9\%$. The duration of the elevated even THD during event 4 is 30–40 min (with 10-min sampling) over the time period 12:20 to 12:50 UT, which agrees well with the timing of the VLF broadband observations of harmonics, shown earlier.

The observations during this period demonstrate evidence of transformer stress (through generated harmonics) linked to the magnitude of GIC due to changes in the local magnetic field. The data presented in this study are consistent with existing indirect evidence that geomagnetic storms impact electrical network performance in New Zealand. A study examining ~ 4 years of New Zealand real-time wholesale electricity prices and geomagnetic disturbances concluded that the “standard deviation in the nodal price, a measure of energy losses and transmission constraints, is more likely to be large when the GIC proxy is large” (Forbes & St. Cyr, 2008). The study reported that real-time market conditions for power grids in multiple locations around the world were statistically related to geomagnetic disturbances (a GIC proxy) and that this effect was strongly seen in the New Zealand data.

5. Summary and Discussion

In this study we have analyzed the effects of a geomagnetically disturbed period on the HWB substation located in Dunedin, New Zealand. There was unprecedented data coverage from a unique set of instruments, that is, measurements of GIC effects on the T4 transformer housed within HWB, magnetic field measurements from a magnetometer located only 7 km from HWB, VLF wideband measurements at, and near, HWB detecting the presence of power system harmonics, and voltage distortion measurements made on a 110-kV line circuit breaker connected to the T4 transformer.

During 6 and 7 September 2017 two interplanetary solar wind shocks occurred, generating four distinct periods of GIC. The two shock events produced very different levels of disturbance, probably due to the orientation of the vertical component of the IMF, B_z . Both shocks were closely associated in time with short-lived spikes in GIC, and were followed by declining effects over 6–10 hr consistent with the effects of geomagnetic pulsations, but neither shock generated any observable harmonics at HWB, indicating that the substation transformers were not significantly stressed by the events, even though T4 reported a short-duration peak GIC of 34 A during the second shock event.

However, two periods of substorm activity generated longer-lasting GIC in T4, with harmonic distortion detected from the substation when GIC levels exceeded about 15 A. The observations indicated that half-wave saturation of the transformer occurred continuously for 30 min during the most effective substorm. VLF receiver systems picked up harmonics up to the thirtieth harmonic, with only specific harmonics enhanced possibly due to in-line impedance resonances in the transmission system. The VLF harmonic observations were consistent with increases in even harmonic THD detected on a connecting 110-kV line, which occurred coincidentally with small decreases in odd harmonic THD.

The substorm periods showed better agreement between T4 GIC variations and nearby Swampy Summit magnetometer data, than for the more distant Middlemarch and EYR magnetometer data. This suggests that small-scale ionospheric currents were important in the substation response to geomagnetic activity levels. However, for the global-scale solar wind shock events, data from all three magnetometer sites (Swampy Summit, Middlemarch, and EYR) showed similar temporal behavior to the relative variations of the HWB T4 GIC.

Acknowledgments

This research was supported by the New Zealand Ministry of Business, Innovation and Employment Hazards and Infrastructure Research Fund contract UOOX1502. The authors would like to thank Transpower New Zealand for supporting this study. EYR magnetometer data availability is described at http://www.intermagnet.org/imos/imos-list/imos-details-eng.php?iaga_code=EYR. Suomi NPP VIIRS data are available from <http://ftp-npp.class.ngdc.noaa.gov>. The authors of this study extend thanks to all VIIRS SDR and EDR team members for their hard work validating and ensuring VIIRS SDR data quality. The New Zealand LEM DC data from which we determined GIC measurements were provided to us by Transpower New Zealand with caveats and restrictions. This includes requirements of permission before all publications and presentations. In addition, we are unable to directly provide the New Zealand LEM DC data or the derived GIC observations. Requests for access to the measurements need to be made to Transpower New Zealand. At this time the contact point is Michael Dalzell (michael.dalzell@transpower.co.nz). We are very grateful for the substantial data access they have provided, noting this can be a challenge in the Space Weather field (Hapgood & Knipp, 2016). We would also like to thank Wayne Cleaver of Electrix Limited for their assistance in facilitating the VLF measurements at Halfway Bush. Middlemarch magnetometer data are available at CRUX magnetometer array website (<http://www1.osakac.ac.jp/crux/>). Swampy Summit magnetometer data are available at <http://auroraalert.otago.ac.nz/quicklooks/magnetometer/>. The VLF data from Halfway Bush and Swampy Summit sites for 7 and 8 September 2017 can be found at <https://zenodo.org/record/1246869#.WvoINXWFOk5>. DSCOVR data can be found at https://www.ngdc.noaa.gov/dscovr/portal/index.html#. Dst and Wp data are available at <http://wdc.kugi.kyoto-u.ac.jp/wdc/Sec3.html>. MAC would like to acknowledge support for this work from the Natural Environment Research Council, NERC NE/P017231/1: Space Weather Impacts on Ground-based Systems (SWIGS).

References

- Albertson, V. D., Bozoki, B., Feero, W. E., Kappenman, J. G., Larsen, E. V., & Nordell, D. E. (1992). Geomagnetic disturbance effects on power systems. *IEEE Transactions on Power Delivery*, 8(3), 1206–1216.
- Béland, J., & Small, K. (2004). Space weather effects on power transmission systems: The cases of Hydro-Québec and Transpower New Zealand Ltd. In I. A. Daglis (Ed.), *Effects of space weather on technological infrastructure* (pp. 287–299). Netherlands: Kluwer Acad.
- Birkeland, K. (1908). *Norwegian Aurora Polar Expedition, 1902–3 Part 1*. Christiania: H. Aschehoug and Company.
- Boteler, D. H., Pirjola, R. J., & Nevanlinna, H. (1998). The effects of geomagnetic disturbances on electrical systems at the Earth's surface. *Advances in Space Research*, 22(1), 17–27. [https://doi.org/10.1016/S0273-1177\(97\)01096-X](https://doi.org/10.1016/S0273-1177(97)01096-X)
- Boteler, D. H., Shier, R. M., Watanabe, T., & Horita, R. E. (1989). Effects of geomagnetically induced currents in the BC Hydro 500 kV system. *IEEE Transactions on Power Delivery*, 4(1), 818–823. <https://doi.org/10.1109/61.19275>
- Butala, M. D., Kazerooni, M., Makela, J. J., Kamalabadi, F., Gannon, J., Zhu, H., & Overbye, T. J. (2017). Modeling geomagnetically induced currents from magnetometer measurements: Spatial scale assessed with reference measurements. *Space Weather*, 15, 1357–1372. <https://doi.org/10.1002/2017SW001602>
- Carroll, D. P., Kasturi, S., Subudhi, M., & Gunther, W. (1993). Harmonic effects of solar geomagnetically induced currents on the electrical distribution system in nuclear power plants. Brookhaven National Laboratory report, BNL-NUREG-48242. Retrieved from http://www.iaea.org/inis/collection/NCLCollectionStore/_Public/24/054/24054574.pdf?r=1
- Cliilverd, M. A., Rodger, C. J., Dietrich, S., Raita, T., Ulich, T., Clarke, E., et al. (2010). High-latitude geomagnetically induced current events observed on very low frequency radio wave receiver systems. *Radio Science*, 45, RS2006. <https://doi.org/10.1029/2009RS004215>
- Cliilverd, M. A., Rodger, C. J., Thomson, N. R., Brundell, J. B., Ulich, T., Lichtenberger, J., et al. (2009). Remote sensing space weather events: Antarctic-Arctic Radiation-belt (Dynamic) Deposition-VLF Atmospheric Research Consortium network. *Space Weather*, 7, S04001. <https://doi.org/10.1029/2008SW000412>
- Cummings, W. D., & Dessler, A. J. (1967). Field-aligned currents in the magnetosphere. *Journal of Geophysical Research*, 72, 1007–1013. <https://doi.org/10.1029/JZ072i003p01007>
- Divett, T., Ingham, M., Beggan, C. D., Richardson, G. S., Rodger, C. J., Thomson, A. W. P., & Dalzell, M. (2017). Modeling geoelectric fields and geomagnetically induced currents around New Zealand to explore GIC in the South Island's electrical transmission network. *Space Weather*, 15, 1396–1412. <https://doi.org/10.1002/2017SW001697>
- Fiori, R. A. D., Boteler, D. H., & Gillies, D. M. (2014). Assessment of GIC risk due to geomagnetic sudden commencements and identification of the current systems responsible. *Space Weather*, 12, 76–91. <https://doi.org/10.1002/2013SW000967>
- Forbes, K. F., & St. Cyr, O. C. (2008). Solar activity and economic fundamentals: Evidence from 12 geographically disparate power grids. *Space Weather*, 6, S10003. <https://doi.org/10.1029/2007SW000350>
- Gaunt, C. T., & Coetzee, G. (2007). Transformer failures in regions incorrectly considered to have low GIC risk. Power Tech, 2007 IEEE Lausanne. 807–812. <https://doi.org/10.1109/PCT.2007.4538419>
- Girgis, R. S., & Vedante, K. B. (2015). Impact of GICs on power transformers. *IEEE Electrification Magazine*.
- Gish, W. G., Palitti, A., Feero, W. E., & Whittemore, T. R. (1995). SUNBURST GIC Network—Phase II progress report. December 1995.
- Hapgood, M., & Knipp, D. J. (2016). Data citation and availability: Striking a balance between the ideal and the practical. *Space Weather*, 14, 919–920. <https://doi.org/10.1002/2016SW001553>
- Hayashi, K., Oguti, T., Watanabe, T., Tsuruda, K., Kokubun, S., & Horita, R. E. (1978). Power harmonic radiation enhancement during the sudden commencement of a magnetic storm. *Nature*, 275(5681), 627–629. <https://doi.org/10.1038/275627a0>
- IEEE Std 519-2014 (2014). IEEE recommended practice and requirements for harmonic control in electric power systems. IEEE Std 519–2014 (Revision of IEEE Std 519–1992) pp. 1–29.
- Joselyn, J. A., & Tsurutani, B. T. (1990). Geomagnetic Sudden impulses and storm sudden commencements: A note on terminology. *Eos, Transactions of the American Geophysical Union*, 71(47), 1808. <https://doi.org/10.1029/90EO00350>
- Kappenman, J. G. (1996). Geomagnetic storms and their impact on power systems. *IEEE Power Engineering Review*, 16(5), 5.
- Mac Manus, D. H., Rodger, C. J., Dalzell, M., Thomson, A. W. P., Cliilverd, M. A., Petersen, T., et al. (2017). Long term geomagnetically induced current observations in New Zealand: Earth return corrections and geomagnetic field driver. *Space Weather*, 15, 1020–1038. <https://doi.org/10.1029/2017SW001635>
- Marshall, R. A., Dalzell, M., Waters, C. L., Goldthorpe, P., & Smith, E. A. (2012). Geomagnetically induced currents in the New Zealand power network. *Space Weather*, 10, S08003. <https://doi.org/10.1029/2012SW000806>
- Martin, B. R. (2012). *Statistics for physical science*. Heindl: Academic Press. <https://doi.org/10.1016/B978-0-74012-387760-4.00010-X>
- Molinski, T. S. (2002). Why utilities respect geomagnetically induced currents. *Journal of Atmospheric and Solar-Terrestrial Physics*, 64(16), 1765–1778. [https://doi.org/10.1016/S1364-6826\(02\)00126-8](https://doi.org/10.1016/S1364-6826(02)00126-8)
- Mollman, A., & Pahlavanpour, B. (1999). New guidelines for interpretation of dissolved gas analysis in oil-filled transformers. *Electra*, 186, 30–51.
- Němec, F., Santolík, O., Parrot, M., & Berthelier, J. J. (2006). Power line harmonic radiation (PLHR) observed by the DEMETER spacecraft. *Journal of Geophysical Research*, 111, A04308. <https://doi.org/10.1029/2005JA011480>
- Nosé, M., Iyemori, T., Wang, L., Hitchman, A., Matzka, J., Feller, M., et al. (2012). Wp index: A new substorm index derived from high-resolution geomagnetic field data at low latitude. *Space Weather*, 10, S08002. <https://doi.org/10.1029/2012SW000785>
- Obana, Y., Waters, C. L., Sciffer, M. D., Menk, F. W., Lysak, R. L., Shiokawa, K., et al. (2015). Resonance structure and mode transition of quarter-wave ULF pulsations around the dawn terminator. *Journal of Geophysical Research: Space Physics*, 120, 4194–4212. <https://doi.org/10.1002/2015JA021096>
- Oughton, E. J., Skelton, A., Horne, R. B., Thomson, A. W. P., & Gaunt, C. T. (2017). Quantifying the daily economic impact of extreme space weather due to failure in electricity transmission infrastructure. *Space Weather*, 15, 65–83. <https://doi.org/10.1002/2016SW001491>
- Pirjola, R. J., & Boteler, D. (2017). Truncation of the earth impulse responses relating geoelectric fields and geomagnetic field variations. *Geoscience Research*, 2. <https://doi.org/10.22606/gr.2017.22002>
- Preacher, K. J. (2002). Calculation for the test of the difference between two independent correlation coefficients [Computer Software]. Retrieved from <http://quantpsy.org>
- Pulkkinen, A., Lindahl, S., Viljanen, A., & Pirjola, R. (2005). Geomagnetic storm of 29–31 October 2003: Geomagnetically induced currents and their relation to problems in the Swedish high-voltage power transmission system. *Space Weather*, 3, S08C03. <https://doi.org/10.1029/2004SW000123>
- Pulkkinen, A., Thomson, A., Clarke, E., & McKay, A. (2003). April 2000 geomagnetic storm: Ionospheric drivers of large geomagnetically induced currents. *Annales Geophysicae*, 21(3), 709–717.

- Ramírez-Niño, J., Haro-Hernández, C., Rodríguez-Rodríguez, J. H., & Mijarez, R. (2016). Core saturation effects of geomagnetic induced currents in power transformers. *Journal of Applied Research and Technology*, *14*(2), 87–92. <https://doi.org/10.1016/j.jart.2016.04.003>
- Rodger, C. J., Mac Manus, D. H., Dalzell, M., Thomson, A. W. P., Clarke, E., Petersen, T., et al. (2017). Long-term geomagnetically induced current observations from New Zealand: Peak current estimates for extreme geomagnetic storms. *Space Weather*, *15*, 1447–1460. <https://doi.org/10.1002/2017SW001691>
- Thomson, A. W. P., Dawson, E. B., & Reay, S. J. (2011). Quantifying extreme behavior in geomagnetic activity. *Space Weather*, *9*, S10001. <https://doi.org/10.1029/2011SW000696>
- Viljanen, A., Nevanlinna, H., Pajunpää, K., & Pulkkinen, A. (2001). Time derivative of the horizontal geomagnetic field as an activity indicator. *Annales Geophysicae*, *19*(9), 1107–1118.
- Wallis, D. D., Anger, C. D., & Rostoker, G. (1976). The spatial relationship of auroral electrojets and visible aurora in the evening sector. *Journal of Geophysical Research*, *81*, 2857–2869. <https://doi.org/10.1029/JA081i016p02857>
- Werner, S. W., Rodger, C. J., & Thomson, N. R. (2005). Identifying power line harmonic radiation from an electrical network. *Annales Geophysicae*, *23*(6), 2107–2116.
- Yearby, K. H., Smith, A. J., Kaiser, T. R., & Bullough, K. (1983). Power line harmonic radiation in Newfoundland. *Journal of Atmospheric and Terrestrial Physics*, *45*(6), 409–419.